Neuroscience 144 (2007) 604–615

DEVELOPMENT OF A HIGH RESOLUTION THREE-DIMENSIONAL SURGICAL ATLAS OF THE MURINE HEAD FOR STRAINS 129S1/SvImJ AND C57Bl/6J USING MAGNETIC RESONANCE IMAGING AND MICRO-COMPUTED TOMOGRAPHY

E. CHAN,[a1] N. KOVACEVÍC,[b1] S. K. Y. HO,[a] R. M. HENKELMAN[b] AND J. T. HENDERSON[a]*

[a]*Department of Pharmaceutical Sciences, Leslie Dan Faculty of Pharmacy, University of Toronto, Room 903, 144 College Avenue, Toronto, ON, Canada M5S 3M2*

[b]*Mouse Imaging Centre, Hospital for Sick Children, 555 University Avenue, Toronto, ON, Canada M5G 1X8*

Abstract—The mouse has emerged as a major experimental model system for examining the functional properties of the mammalian CNS; both during development and following CNS injury. Histologic procedures currently used to determine the relative position of structures within the CNS are presently limited in their ability to take full advantage of this system for surgical and morphometric procedures. We present here the first three-dimensional interactive digital atlas of the murine brain and skull for two genetically important strains of mice; 129S1/SvImJ and C57Bl/6J. The final resolution of these digital atlases is 54 μm^3. These representations of the murine brain and skull, in conjunction with our development of a new, more dynamic master coordinate system, provide improved accuracy with respect to targeting CNS structures during surgery compared with previous systems. The interactive three-dimensional nature of these atlases also provide users with stereotactic information necessary to perform accurate "off-axis" surgical procedures, as is commonly required for experiments such as *in vivo* micro-electroporation. In addition, three-dimensional analysis of the brain and skull shape in C57Bl, 129Sv, CD1, and additional murine strains, suggests that a stereotactic coordinate system based upon the lambda and rostral confluence of the sinuses at the sagittal midline, provides improved accuracy compared with the traditional lambda–bregma landmark system. These findings demonstrate the utility of developing highly accurate and robust three-dimensional representations of the murine brain and skull, in which experimental outputs can be directly compared using a unified coordinate system. The aim of these studies is to enhance comparative morphometric analyses and stereotactic surgical procedures in mice.

Key words: imaging, mouse, brain, anatomy, transgenic, knockout.

Increasingly, mice are utilized as a primary model system to elucidate the mechanisms by which mammalian genes and genetic networks regulate physiologic and morphologic processes. The ability to make specific modifications to the murine genome, together with sequencing of the entire genome for several murine strains, has greatly facilitated these actions and promoted the use of mice in a variety of high-throughput morphologic screens. These developments have stimulated the need for more rapid, more sensitive means of quantitatively analyzing differences in features such as structural morphology. Neuroanatomic and morphometric analyses of the murine brain and skull would be greatly assisted by the development of a robust, unified three-dimensional (3D) coordinate system for the murine head, in which scaled outputs of analyses performed among different animals in different strains could be directly compared. Using such a system, neuroanatomic attributes within these strains could be analyzed in a quantitative manner. Without such a coordinate system, there exists no common basis to compare 3D data sets generated in different research centers. Previously, we have discussed the rationale and methodology involved in developing 3D image registration and analysis procedures (Kovačević; et al., 2004). In the present study we develop for general scientific use, spatially accurate 3D representations of the murine brain and skull of two important murine lineages; and discuss the rationale for implementation of a new more robust stereotactic coordinate system. Quantitative and comparative analyses performed using this system indicate that it is significantly less prone to stereotactic placement errors due to strain/specimen-specific deviations in skull geometry; thus producing more accurate and reproducible stereotactic placements.

As indicated above, rapid advancement in the ability to produce and map complex quantitative trait loci (QTL's) among inbred murine strains has stimulated the need for more accurate and sensitive means of performing quantitative morphologic comparisons. Traditionally these comparisons have been made using histology on 2D sections. While traditional histologic atlases are advantageous due to their high spatial resolution (~2 μm), the procedures involved in interpolating 3D structures from these data preclude them from providing highly accurate volumetric or positional coordinate information (Rogers et al., 1990; Santori and Toga, 1993; Kaufman et al., 1998). The difficulty in accurately reconstructing 3D structures is primarily due to variations arising from individual 2D layers of the ultimate 3D stack. These errors may arise from a number of sources, but in histologic sections typically arise during the process of tissue preparation (dehydration/re-hydra-

[1] Authors contributed equally to this work.

*Corresponding author. Tel: +1-647-880-1521; fax: +1-416-978-8511.
E-mail address: jeff.henderson@utoronto.ca (J. T. Henderson).

Abbreviations: CR, Charles River; CT, computed tomography; GPS, global positioning system; JL, Jackson Laboratories; lbd, lambda to bregma distance; MRI, magnetic resonance imaging; PBS, phosphate buffer; PFA, paraformaldehyde; 3D, three-dimensional.

0306-4522/07$30.00+0.00
doi:10.1016/j.neuroscience.2006.08.080

tion), sectioning (non-random physical distortion), or subsequent handling procedures (mounting deformation, etc.). The direction of this introduced error (i.e. expansion, contraction, distortion) may or may not be similar in successive sections, but will be compounded in the resulting z-dimension stack. While a number of robust morphologic rendering programs have been developed to minimize distortion and optimize serial section alignment, the fundamental limitation in these procedures is that there is no means to objectively determine which section or localized region within a given alignment represents the true orientation of the structure being analyzed. Since it is difficult to ensure with certainty that processing errors do not affect all sections to some extent, it can be argued that neither element of a given alignment may accurately represent the resulting z-structure.

This fundamental limitation has been increasingly overcome in recent years through the use of imaging techniques which examine the structure of interest in its entirety. A clear tradeoff in this approach is the maintenance of acceptable levels of spatial resolution within the structure analyzed. With respect to techniques such as magnetic resonance imaging (MRI), in recent years magnetic field strengths have increased such that spatial resolutions of 30–60 μm^3 can now be obtained. In the present study, we have utilized high-resolution MRI in combination with micro-computed tomography (CT) to directly capture 3D information for the murine brain and skull. While the spatial resolution provided by these techniques is significantly less than that obtained using traditional histology (54 μm isotropic resolution for MRI, 38 μm isotropic resolution for micro-CT), little to no sample processing is required to analyze these tissues; thus reducing this important source of error. As MR and CT imaging allow visualization of structures in their entirety, there is no need for post-reconstruction of sectioned samples. Again, this provides a substantial advantage with respect to the reliability of the 3D spatial estimates obtained. Consistent with this, several groups in recent years have performed MRI (Benveniste et al., 2000; Johnson et al., 2002; Natt et al., 2002; Chen et al., 2005) imaging of the rodent nervous system, and atlases of individual murine brains for several strains of mice have been produced (Dhenain et al., 2001; MacKenzie-Graham et al., 2003; Koshibu et al., 2004; Kovacevic et al., 2005; MacKenzie-Graham et al., 2004, see also http://mouseimaging.bioinfo.sickkids.on.ca/var_brain_atlas.html). While techniques such as MRI are superior with respect to visualizing the soft tissues of the CNS (Munasinghe et al., 1995; Natt et al., 2002), techniques such as CT are better suited to imaging calcified structures such as the murine skull (Ford-Hutchinson et al., 2003; Boone et al., 2004; Recinos et al., 2004).

While high-resolution MR images of murine brains produced by our and other groups are informative with respect to the direct visualization of CNS structures, they are of limited utility for stereotactic/surgical procedures, which require a spatially accurate coordinate system based upon visible (e.g. external) landmarks. To develop such an atlas, its is necessary to perform both MR and micro-CT imaging on an individual specimen, which has previously been selected based upon morphologic criteria to represent an "average" individual from the population under study. Thus, using MR and micro-CT imaging, we set out to develop a 3D interactive atlas of the murine head for several different strains of genetically important mice. To date, no such atlas of the murine brain/skull has yet been produced for any strain of rodent. Several seminal 2D stereotactic atlases of isolated mouse and rat brains have been previously produced (Slotnik and Leonard, 1975; Paxinos and Watson, 1986; Ghosh et al., 1994; Franklin and Paxinos, 1997) based upon compiled histologic data, and more recently MRI atlases of individual murine brains have been published (Ghosh et al., 1994; Kovacevic et al., 2005; MacKenzie-Graham et al., 2004). The information from these atlases has for many years served as an important foundation for the development of stereotactic surgical procedures performed in rat and mouse. However for these atlases, the relationship between the brain and the external landmarks is indirectly inferred.

Historically, stereotactic placements within the murine CNS have been performed based upon coordinates derived from two key structural landmarks of the skull, the sagittal aspect of the lambda and bregma sutures. In the event of significant deviation in the lambda to bregma distance (lbd, see Fig. 1 for overview of skull landmarks) between a given experimental animal and the atlas standard, a scalar correction of the derived x, y and z coordinates was performed. Such procedures are typically assumed to provide a reasonable estimate of the position of major structures within the CNS, provided that the atlas used and the specimens are derived from similar genetic backgrounds. In the event that a given placement misses the intended target, subsequent rounds of experimentation can ultimately provide the correct coordinates for a given procedure. However, such procedures can be both time consuming and costly, particularly in the case of complex genetic models involving multiple gene modifications. In addition, our analysis of inbred and outbred murine strains, indicates that there are substantial non-linear, non-isotropic differences in the morphology of the brain and skull among these groups. These differences extend to the relative intracranial position of CNS structures and neural loci with respect to external landmarks. For these reasons, we have sought to develop strain-specific interactive stereotactic atlases for several genetically important strains of mice. Consistent with this, the strains C57Bl/6J and 129S1/SvImJ represent murine lineages whose genomes have been completely sequenced at present. C57Bl/6J is perhaps the most thoroughly studied strain of mice with respect to neurologic mutations, and represents a principle backcross strain for new induced mutations for major mouse breeders such as Jackson laboratories. 129Sv represents the primary strain from which the large majority of embryonic stem cells are derived. As such 129Sv represents the primary genetic background for the generation of new lines of genetically modified mice. The development of accurate 3D stereotactic atlases for these strains would therefore be of benefit to a wide variety of neurologic investigations.

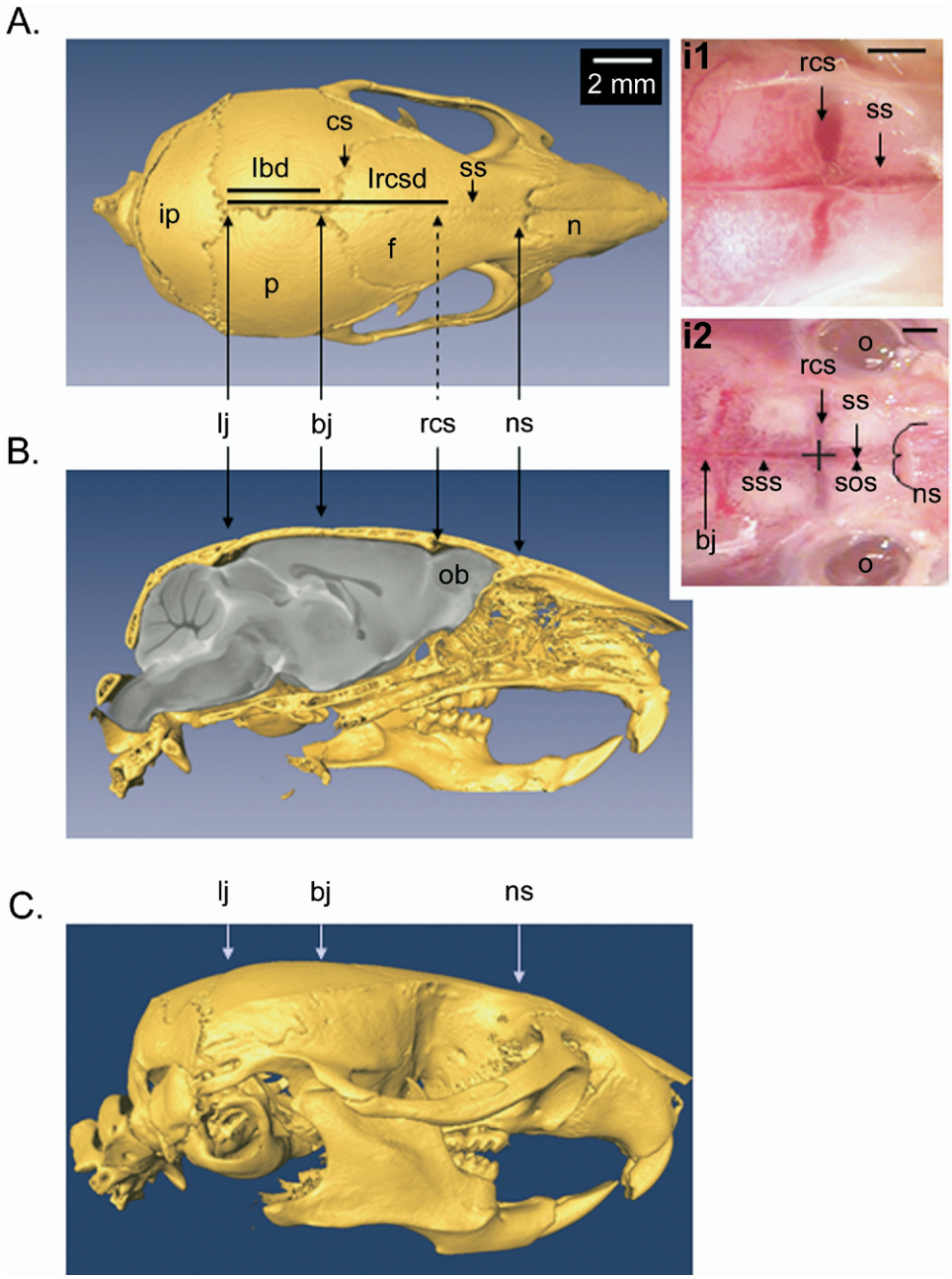

Fig. 1. Overview of major cerebral landmarks of murine skull. Shown in A–C are CT/MRI representations of the mouse cerebrum. Schematics are oriented such that caudal aspects of the skull show to the left, rostral aspects to the right. (A) Dorsal view of the skull showing major landmarks with scale bar; (B) split sagittal view; (C) lateral view. Inset 1: photomicrograph of the surgical appearance of the rostral aspect of the dorsal skull following dissection. Position of the rostral confluence of the sinus (rcs, visible through the skull in all strains examined), and sagittal suture (ss) are indicated. Scale bar=1 mm. Inset 2: photomicrograph of denuded dorsal skull indicating positions of adjacent anatomic structures. Intersection of rcs and ss (cross) represents new rostral landmark used for stereotactic placements; (o), orbit, (ns), nasal suture, the junction of the nasal (n) and frontal (f) bones, rcs, the junction point at which the superior sagittal sinus (sss) meets the superior olfactory sinus (sos) at the sagittal midline, (ob) olfactory bulb, (bj)–bregma junction, junction of the f and parietal plates at the sagittal suture (this point can also defined as the junction of the coronal and sagittal sutures). Scale bar=1 mm. Additional abbreviations: lj, lambda junction, juncture of the parietal (p) and inter-parietal (ip) plates at the sagittal suture; lbd, a common landmark used for stereotactic surgery; lrcsd, lambda to rcs distance, proposed improvement to stereotactic landmark system.

EXPERIMENTAL PROCEDURES

Animals and tissue preparation

Eight-week old inbred 129S1/SvImJ (Jackson Laboratories [JL], Bar Harbor, ME, USA), C57Bl/6J (Charles River Laboratories, Inc. [CR], Wilmington, MA, USA) and outbred CD1 (CR) or ICR (JL) male mice were obtained from either JL or CR and housed in our gnotobiotic animal colony for 72 h following arrival. Individuals for additional strain comparisons (BALB/cJ, C57BL/6J, DBA/2J, A/J, FVB/NJ, C3H/HeJ) were also obtained from JL or from our own

colony at the Samuel Lunenfeld Research Institute, Mount Sinai Hospital, Toronto. At the time of kill, mice were anesthetized with tri-bromoethanol (Avertin^{R} 250 mg/kg). Following a lack of deep tendon responses, the thoracic cavity was opened and animals were perfused through the left ventricle with 10 ml of 0.1 M phosphate buffer (pH 7.4), 0.9% NaCl (PBS), followed immediately by 4% paraformaldehyde in 0.1 M PBS (PFA) at 25 °C. Brains were then post-fixed overnight within the skull in PFA at 25 °C. Following fixation, heads were oriented and held in place in the imaging tube through the use of 3% PFA-equilibrated agarose. All procedures performed conformed to University of Toronto and NIH animal care guidelines and were conducted with the aim of minimizing the number of animals used and any acute discomfort. Where histologic examination of the whole brain/skull was performed, heads were first decalcified in a solution of 10% formic acid at 4 °C for 5–7 days, followed by washing and equilibration in 30% sucrose, then frozen sectioned at 50 μm.

Low resolution MRI

Murine heads were initially scanned at a resolution of 121 μm using a 7.0-T magnet (Magnex Scientific, Oxford, UK) with a 3 cm diameter coil, connected to a Unity^{INOVA} console (Varian Instruments, Palo Alto, CA, USA). The parameters used for scans were as follows: T2-weighted, 3D spin-echo sequence, with TR/TE=1660/30 ms, single average, field of view=32×16×16 mm and matrix size=264×132×132, giving an isotropic resolution of 121 μm.

High resolution MRI of isolated brains

Prior to imaging, brains were carefully removed from the surrounding skull and placed into glass tubes filled with a proton-free susceptibility-matching fluid (Fluorinert FC-77, 3M Corporation, St. Paul, MN, USA). The sample was placed in an over-wound solenoid with a diameter of 12 mm and a length of 14 mm. Isolated brains were scanned using the instrumentation indicated above. The parameters used for scans were as follows: T2-weighted, 3D spin-echo sequence, with TR/TE=1600/35 ms, single average, field-of-view=12×12×24 mm and matrix size=200×200×400 giving an image with (54 μm)^3 isotropic voxels. The total imaging time was 18.5 h. The TR and TE settings were chosen for optimized contrast between gray matter and white matter in the mouse brain at seven Tesla as reported in previous studies (Guilfoyle et al., 2003).

High resolution micro-CT imaging

Following low resolution imaging, murine heads were scanned by micro-CT using a MS-8 system, at 80 kVp and 80 μA. For each sample, 905 views were obtained, averaging three frames per view, using 1×1 binning. Additional parameters were as follows: angle of increment 0.4, exposure time 2 s, source to detector distance: 236 mm, source to object distance: 118 mm, CCD detector spacing: 35 μm.

Image preparation

Images present were analyzed and rendered using either the MR software package Display (Montreal Neurological Institute, Montreal, Canada), MICeView (MICe, Hospital for Sick Children, Toronto, Canada) or Amira (TGS, San Diego, CA, USA).

RESULTS

Low resolution MRI of the murine head

As a first step toward generating 3D atlases of the murine head, whole heads of eight week old 129S1/SvImJ or C57Bl/6J male mice were imaged with MR at a resolution of 121 μm immediately following tissue preparation (see Experimental Procedures) and removal of external skin. To prevent movement of the sample within the imaging coil, heads were placed in 3% solidified PFA-agarose. For these experiments, MR contrast of the spin echo pulse sequence was adjusted to maximize visualization of both brain and skull. For both 129S1/SvImJ and C57Bl/6J strains, several individual specimens were imaged, and those samples judged to best represent an average individual from their respective strains were utilized for further analysis (see below). Examples of the data obtained from these imaging studies are shown in Fig. 2A. As indicated in the figure, the parameters used for these imaging studies allowed good visualization of the basic features of the brain, skull, and surrounding musculature. As described below, the low resolution MR data sets provided an important spatial crosscheck for the data derived from subsequent high-resolution MR and micro-CT imaging studies.

High-resolution imaging of murine head

Following initial MRI, samples were scanned via CT at a resolution of 38 μm. Examples of the data obtained are shown in Fig. 2B. CT imaging provided a high resolution map of the morphology of the bony structures of the murine skull, including suture junctions. Immediately following the collection of micro-CT data, murine heads were removed from agarose, and whole brains carefully dissected from surrounding cranial tissues. Isolation of brains provided a smaller sample cross-section, allowing imaging coils to be used which had a better signal to noise ratio. This in turn allowed brains to be imaged at a higher final MR resolution (54 μm). Imaging of brains at this resolution, significantly increased the level of structural detail which could be delineated within the CNS (Fig. 2C) compared with initial cranial scans (Fig. 2A).

Integration of high-resolution MRI and CT data sets

To maximize the structural detail of the final stereotactic atlases, we integrated information obtained from two complementary high-resolution scans: micro-CT of individual heads (Fig. 2B) with high resolution MRI of the excised brain (Fig. 2C). A necessary step for the integration of these data is spatial alignment. As these datasets share no common structures which could potentially be used as landmarks for direct alignment, we utilized the low-resolution MR scans of the whole head (Fig. 2A) as a reference for integrating these data, since it possesses sufficient contrast to observe features of both the brain and skull. We first performed manual registration of the micro-CT and low-resolution MRI data using the program Register (Montreal Neurological Institute). Next, we identified several landmarks within the two datasets and used a rigid-body transformation model for the alignment, since both were derived from the same (intact) mouse head. The result of this alignment is shown in Fig. 3A. In this figure, the CT data (shown as hot metal color map) is overlaid upon the low-resolution MR image (gray scale color map). Next, we registered high-resolution MR data with that from the low-

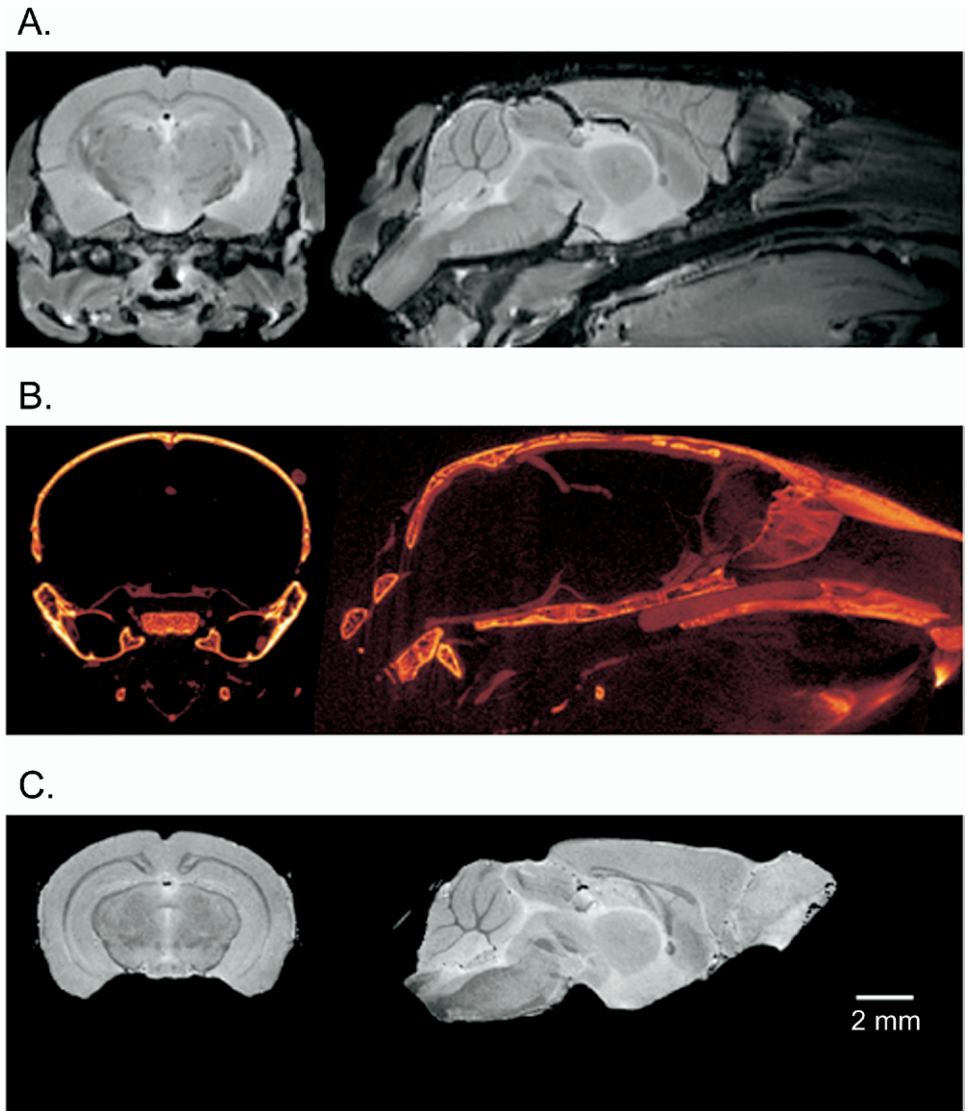

Fig. 2. 3D datasets used for atlas construction. Shown are data collected for a given C57Bl/6J specimen. For each schematic, a coronal view is shown to the left, sagittal view to the right. (A) Dissected whole heads were embedded in isotonic PFA–agarose and subjected to low resolution MRI. (B) Samples were subsequently rescanned using CT, providing greater detail of calcified tissues. (C) Brains were then dissected free from surrounding tissues to enhance high-resolution MRI (voxel size 54 μm).

resolution MR scan (Fig. 3B). In addition to affine (linear) components in this second registration step, fitting of the high resolution MR data onto the low resolution atlas standard also contained non-linear components, as excised brains were labile to non-linear deformation (once free from the supporting structure of the skull, brains have an opportunity to "bend" or "sag" slightly from their original orientation). To do this, we first performed manual registration based on several brain landmarks and a full affine transformation model to achieve the best overall alignment between the two MR images. To account for any further nonlinear deformations, we then used hierarchical, multi-resolution non-liner registration based on maximization of the cross-correlation similarity function. We then combined transforms from the two registration steps to produce the final transformation which allowed correct positioning of the excised high-resolution MR brain within the high-resolution CT skull. These results are shown in Fig. 3B–D. As a final check that the individual brain/skull scans chosen to represent the surgical atlas for a given strain did in fact represent an "average" individual with respect to brain morphology, these composite scans were checked against our previously published variational (average) atlases of (isolated) murine brains for each strain (Chen et al., 2005).

Morphometric comparison of murine strains: factors affecting global orientation

Fig. 4A shows a visualization of several structures within the CNS, derived from data from our previously published variational atlas of the isolated mouse brain. These visualizations, while helpful for neuroanatomic comparisons,

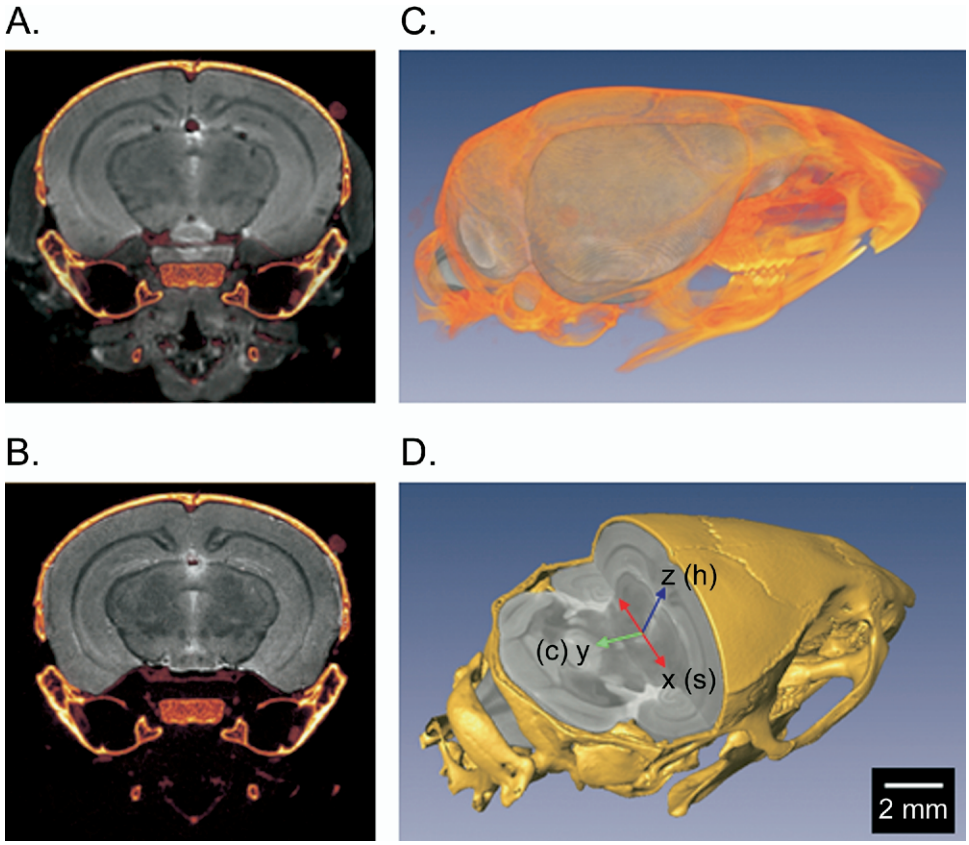

Fig. 3. Construction of interactive atlas dataset. Steps to obtain interactive 3D atlas are shown for a given (C57Bl/6J) dataset. (A) View of high resolution CT image registered upon low resolution MR scan for analysis of spatial integrity. (B) Final registration of high resolution MR and CT scans comprising the final atlas. (C) Transparent 3D overlay of skull upon brain showing exterior cranial landmarks. (D) Cutaway view of brain and skull showing interior details of CNS with axes with scale bar for panels. Movement along the *x*, *y* or *z* axes corresponds to successive sections in the sagittal (s), coronal (c), or horizontal (h) planes respectively.

are not informative for the planning of surgical procedures due to the lack of corresponding external (and thus easily accessible) surgical landmarks. As shown in Fig. 4B, using the combined high resolution MR/CT data, the precise location of CNS structures in different murine strains can now be accurately determined with respect to external landmarks. Using such a system, the position of internal CNS structures can be directly determined in terms of accessible reference points, enhancing the accuracy of stereotactic placements and morphometric measurements in a given specimen. However, the positional stability of any system based upon external landmarks (across individuals or strains) is subject to the morphologic stability of these landmarks relative to the internal CNS structures targeted. Optimizing these general external reference landmarks thus requires a detailed understanding of the variation in cranial morphology which exists in different murine strains.

MRI and histologic analyses of the brain/skull of both inbred (129S1/SvImJ, C57Bl/6J, FVB/N, C3H, DBA) and outbred (ICR, CD1, BalbC, 129/C57 F1 hybrids) mice, indicate that the principal morphometric variable reducing the accuracy of dorsal skull landmarks is tied to variations in cranial curvature along the rostral–caudal (*y*) axis. An example of this is shown in Fig. 5 for male *Mus musculus* C57Bl/6J (green) and 129Sv/ImJ (red) mice whose gross body weight are within 1 g of one another. These scaled comparisons of average individuals from C57Bl/6J and 129S1/SvImJ have been overlaid in such a manner as to maximize superimposition of their cerebrum and demonstrate that these two strains differ significantly with respect to the geometric relationship of their CNS structures to landmarks along the exterior skull. As indicated in the figure, utilization of LCS/lambda versus bregma/lambda landmarks results in more stable and reproducible horizontal angulation among these two disparate murine strains. C57Bl/6J mice (green) exhibit greater curvature in their dorsal skull, and have a greater depth to their cranial vault compared with 129S1/SvImJ mice (red). This difference in cranial structure can also be seen by comparison of Figs. 5 C (C57) and 5D (129Sv). In both, the dotted line along the *y* axis has been positioned such that it intersects with identical suture points within the cranial vault. In addition to differences in overall skull curvature, these strains also exhibit differences in their distribution of neural structures within the CNS, as exemplified by the corpus callosum (Fig. 5C, D; arrowhead). As seen in Fig. 5A, the comparative increase in cranial volume seen in C57Bl versus 129Sv mice is not distributed equally, being greater in the rostral than caudal elements of the brain. While the differ-

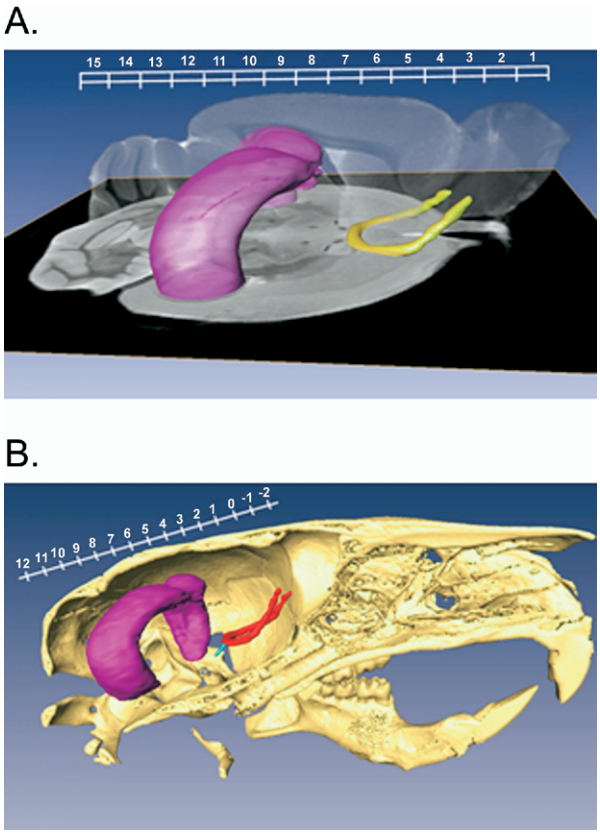

Fig. 4. Stereotactic visualization of CNS structures within the atlas. (A) Off-axis sagittal view of the hippocampi (purple) and the pars anterior of the anterior commissure (yellow) within the brain in relation to surrounding tissues with sagittal and horizontal MR reference planes indicated. Distances along the rostral–caudal (*y*) axis are indicated in terms of absolute values in millimeters. (B) Visualization as in (A) shown in relation to the surrounding skull. This format allows stereotactic positions to be accurately assessed. Positions along the rostral–caudal axis are indicated in millimeters relative to an external fixed landmark (RCS). For view (B), the hippocampus is shown in purple, pars anterior of the anterior commissure in red, and pars posterior of the anterior commissure in teal.

ences in skull shape observed between C57Bl/6J and 129S1/SvImJ mice are nominal compared with the total range of morphometric differences we have observed among other strains, they serve to illustrate the fundamental features which affect the stereotactic accuracy of dorsal landmarks. These findings highlight the importance of using strain-specific stereotactic atlases for both detailed surgical placements and morphologic analyses.

Despite these differences, it is also critical to develop general stereotactic systems and coordinate frameworks which are both robust and stable, so that results obtained from different stains/individuals are as directly comparable as possible with a minimum of artifact. As shown in Fig. 5B, not all dorsal landmarks of the skull showed the same degree of variability. In particular, we observed that the lambda and RCS (a landmark defined by junction of the superior sagittal sinus and superior olfactory sinus) junctures along the sagittal midline exhibited consistently lower levels of positional variability compared with other dorsal landmarks following global alignment of the head. This stability is likely due to their relative position with respect to the geometric centroid of the brain. Consistent with this, landmarks located at the periphery of the brain (rostral–caudal dimension) exhibited greater variability. The bregma also exhibited greater variability than either the lambda or RCS landmarks between strains following linear alignment (Fig. 5B). This may reflect greater susceptibility of the bregma to genetic influences with respect to positional determination compared with the lambda or RCS.

Thus the primary factors which affect the stereotactic reliability among the strains appears to be positional consistency of the landmarks used and stability of *y* axis angulation with respect to internal CNS structures in response to differences in (rostral–caudal) skull curvature. The importance of rostral–caudal angulation makes sense if one considers that strain differences which alter the *x* (lateral) or *z* (dorsal-ventral) axis dimensions do not strongly affect stereotactic alignment as it is practically applied (using dorsal landmarks). Identification of the midsagittal plane is straightforward regardless of the lateral extent or shape of a given specimen (i.e. relative rotation about the *z* axis or "roll" can typically be assessed with high confidence). The same is true regarding dorso-ventral angulation (rotation about the *y* axis or "yaw"), as it is not strongly affected by the "depth" (in the *z* axis) of the specimen. However, because angulation of the *y* axis (i.e. rotation about the *x* axis or "pitch") is defined (for practical reasons) by landmarks which lie along the dorsal aspect of the skull, changes in aspects such as skull curvature can significantly affect *y* axis angulation. Thus carefully defining this parameter is critical, as changes in the angle of the *y* axis alter the interpretation of both the horizontal (XY) and coronal (ZX) planes. Geometrically, the simplest way to reduce the influence of curvature on *y* axis angulation would be to increase the distance between the two primary *y* axis landmarks, and position them such that they lie on either side of the region most prone to curvature effects (parietal and frontal bones of the skull). Thus, ideally one would select two points to determine the *y* axis which are as far apart as possible, at the rostral and caudal ends of the skull. However, the positional consistency of these landmarks among different strains must also be taken into consideration in any general assignment.

Optimization of a general system of cranial landmarks

A robust landmark system should produce global alignments of the murine head which are highly correlated across different strains. To determine the best general stereotactic alignment scheme for the murine head, we examined computational alignments obtained for each of our CT/MR datasets using different cranial landmark combinations. Alignments produced from each of these series were then compared with the global 3D computer alignment of the skull and brain generated using the entire digital data set. Landmark combinations which produced results closest to those obtained from the 3D computer alignments were judged to possess the greatest accuracy.

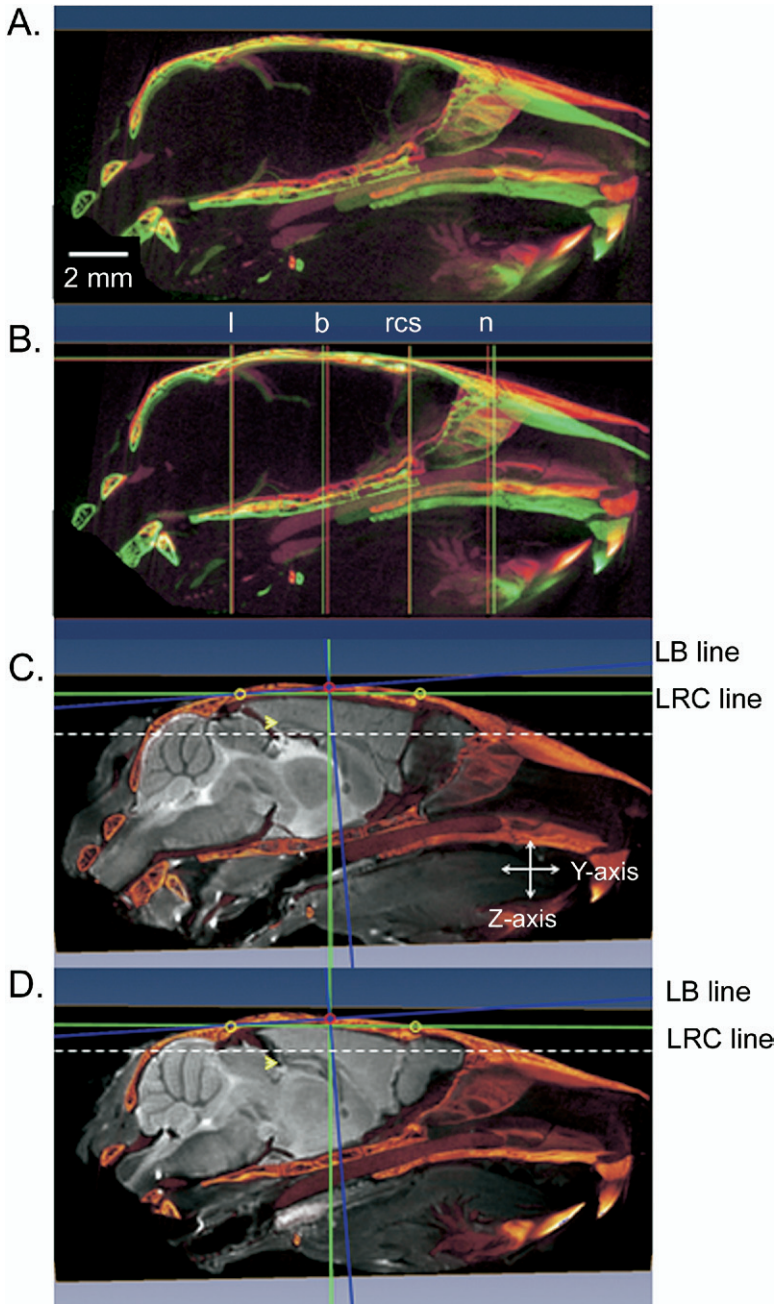

Fig. 5. Comparison of cerebral geometry in C57Bl and 129Sv mice. Shown in (A) and (B) are sagittal overlays of CT skull scans obtained from average C57Bl/6J (green) an 129S1/SvImJ (red) mice. As seen in (A), the skull of C57Bl mice exhibits consistently greater curvature in their dorsal cerebrum and shows greater depth in their cranial vault, compared with age-matched, sex-matched 129Sv mice. In addition, following global alignment of the cerebrum (B), the relative position of several principal morphologic landmarks of the skull (and internal CNS structures; data not shown) differs significantly in C57Bl/6J versus 129Sv/ImJ mice. Abbreviations: l, lambda; b, bregma; rcs, rostral confluence of dorsal sinuses; n, nasal suture. All labels are shown at their point of intersection at the sagittal midline. (C–D) Standardization of murine coordinates across strains. Shown in the figures are MR/CT sagittal views of C57Bl/6J (C) or 129S1/SvImJ (D) murine heads. Lambda, bregma and rcs reference points along the dorsal skull are indicated. The relative stereotactic coordinate frame, based upon either the lambda–rcs, or traditional lambda–bregma landmarks, are indicated by either the LRC (green) or LB (blue) *y* axis lines. As shown in the figure, because the *z* axis is typically defined as being orthogonal to the *y* axis, changes in *y* axis angulation ultimately alter orientation of both the horizontal (XY) and coronal (ZX) planes. For (C) and (D), dotted lines are positioned at similar *z* axis depths within the cranial vault; arrowheads indicate the position of the caudal aspect of the corpus callosum for each strain. These landmarks serve to highlight some of the structural differences encountered among different murine strains. Dimensions for each panel are as indicated in (A).

Analysis of these alignment series demonstrated that the position of the lambda junction is remarkably consistent across the *Mus musculus* backgrounds examined; similar to previous findings (Messier et al., 1999). These results again highlighted the importance of *y* axis angulation in optimizing global alignment among strains and between

individuals; consistent with the findings given above. While each landmark combination produced somewhat different absolute angulations of the *y* axis, the most consistent global alignments were obtained using either lambda–nasal or lambda–RCS landmark pairs (Fig. 5B). Both of these pairs produced alignments which were more consistent than those obtained using lambda–bregma based alignment. The RCS was ultimately utilized as the primary rostral landmark because its greater stability relative to lambda compared with the nasal suture across different murine strains (Fig. 5B). In addition, in surgical practice, use of the nasal suture as a landmark proved less than ideal due to its extreme rostral location. As shown in Fig. 5B, alignments based upon lambda–RCS landmarks produced alignments of the head which were virtually identical to digital alignments of the 3D datasets (digital alignments shown). In addition, these alignments were relatively insensitive to changes in dorsal skull curvature (Fig. 5C, D, composite shown in 5B), and the *y* axis angulation produced using these landmarks (LRC line) orients the brain at a fairly neutral angle (i.e. zero deflection) with respect to the dorsal limit of the cortex.

Defining a unified coordinate system for the murine head

With respect to stereotactic coordinates, delineation of position "0" in the X dimension with respect to the YZ (sagittal) plane is typically straightforward due to the bilateral nature of the brain and skull; with the sagittal midline representing zero. As indicated above, traditionally for surgical procedures in rodents the *y* axis has been defined by the lambda and bregma junctions. Based upon our morphometric analysis of different murine strains, we propose that a more consistent general definition of this parameter would be the point which exists at the dorsal-most aspect of the skull at the lambda and RCS landmarks; as shown in Fig. 6A and B. Using this definition to set the *y* axis angulation (LRC line), establishes the XY (horizontal) reference plane. Determination of *x*- and *y* axis angulation allows *z* axis orientation (and the ZX–coronal plane by extension) to be determined by default, since it is orthogonal to the other two axes. Thus, the lambda and RCS landmarks, together with the bilateral symmetry of the head, define the information required to delineate the three stereotactic reference planes.

Using this system, the "0" position in the horizontal (*z* axis) dimension, corresponds to that XY plane which passed through the dorsal-most aspect of the skull containing the lambda and RCS landmarks (plane represented in Fig. 6B). For the coronal (ZX) plane, assignment of position "0" for the reference plane is somewhat arbitrary. However, we have found it useful for our electronic datasets to identify this coordinate as that plane which passes through the RCS landmark (Fig. 6A). Thus the "0,0,0" (X,Y,Z) coordinate in this system would be the dorsal aspect of the skull which overlies the XY midpoint of the RCS landmark (Fig. 1, inset 2, Fig. 6B, filled circle). With respect to previously published (hard copy) stereotactic atlases, a number of these attempt to present coronal sections in a ZX reference plane which is appropriate for lambda/bregma-based landmarks. Thus by comparison, coronal (and horizontal) sections which are parallel to the reference planes of our atlas will differ in angulation; as shown in Fig. 5C and D. The differences in coronal and horizontal angulation using the lambda–RCS (green lines) versus the previous lambda–bregma (blue lines) varies depending on the strain; but is typically on the order of 3.0–5.0 degrees for the strains examined (129Sv-3.6′, C56Bl6–4.4′). The difference in angulation values seen between 129Sv and C57Bl strains is an indication of the relative susceptibility of the lambda–bregma landmark system to changes in relative position and dorsal skull shape; a finding seen for other strains as well. The development of a unified robust coordinate system for the murine head would allow investigators at disparate sites to directly compare and analyze a variety of morphometric parameters among individuals of a given group (genotype) and across strains. Implementation of such a system would promote a common basis for morphometric comparisons of all aspects of cranial structure for both direct and interpolated (from serial 2D data) 3D data sets. Such data sets are becoming increasingly common as more sophisticated morphologic tools become available. The available distribution file format of the stereotactic atlases developed are MINC, and may be read on any reader which recognizes *.mnc format files. One example of such a freeware 3D reader is Display (Montreal Neurological Institute), http://www.bic.mni.mcgill.ca/software/Display/Display.html. An example of the atlas being utilized using Display is shown in Fig. 6C.

DISCUSSION

Recent enhancements in the resolving capability of non-destructive imaging methods such as magnetic resonance and micro-CT, have allowed us to develop high-resolution (voxel size 54 μm) digital atlases of the murine head. The combined use of MR and CT imaging techniques has allowed us to interactively visualize the brain and skull as a unified whole, improving the accuracy of stereotactic manipulations by directly linking visible landmarks on the dorsal skull to CNS structures. These data provide a significant enhancement in stereotactic control and morphometric comparisons over current 2D slice atlases, none of which presently contains information on skull coordinates. While substantial progress has been made in utilizing MRI to examine the CNS of adult and embryonic mice (Dhenain et al., 2001; Koshibu et al., 2004), at present, no stereotactic MR atlas of the murine brain exists for any strain. We (Chen et al., 2005) and others (Ma et al., 2005) have examined the level of natural variability for structures within the CNS through the generation of probabilistic atlases for strains C57Bl/6J, 129Sv/ImJ, CD1 and C57Bl/6J respectively. In addition, impressive gains have recently been made in the development of a multimodal atlas for the C57Bl/6J mouse brain (MacKenzie-Graham et al., 2004). However in each of these studies, brains were examined in isolation from surrounding tissues, and thus

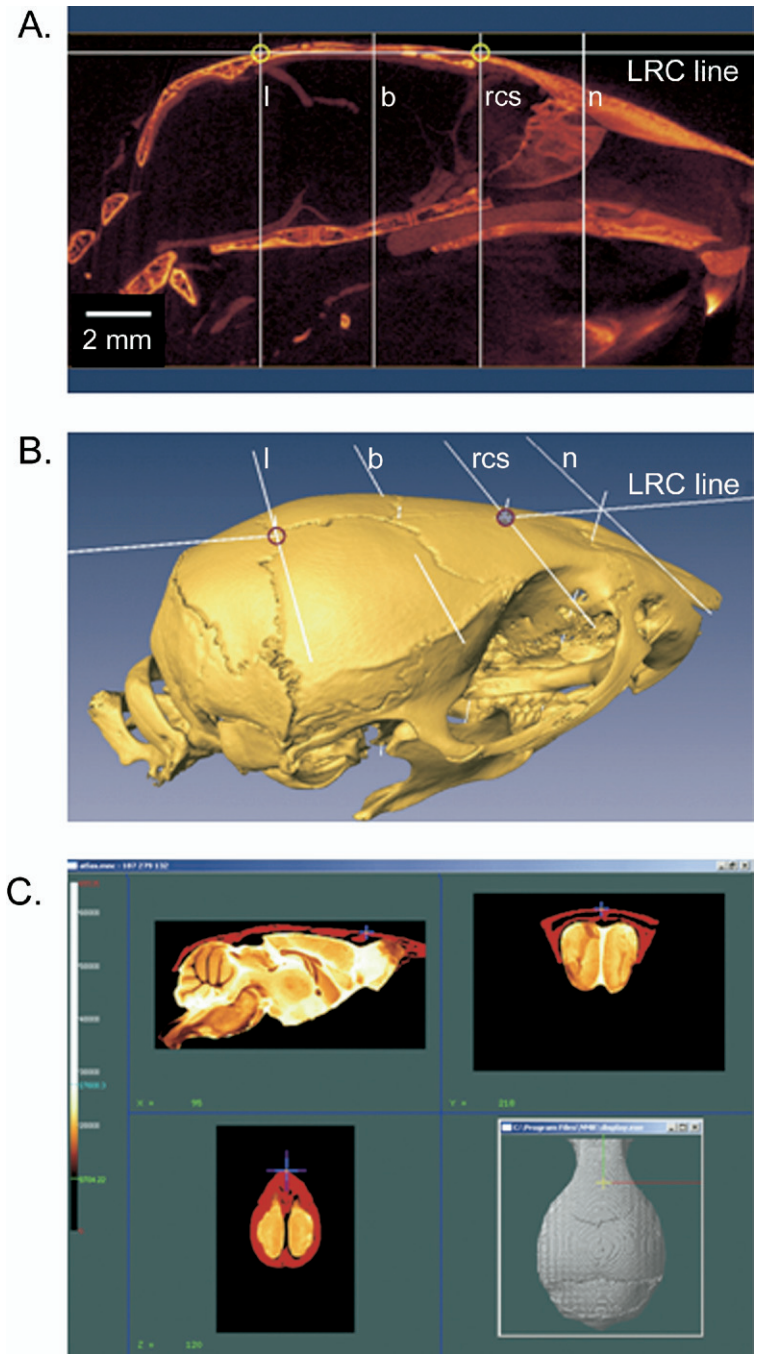

Fig. 6. Alignment definitions for murine atlas. Features used to determine the absolute alignment of murine heads for the stereotactic atlases are illustrated in the following panels. Results are shown for the C57Bl/6J atlas. (A) CT cross-section in the sagittal plane, showing the relative positions of lambda junction and rcs landmarks used to determine the angulation (pitch) of the *y* axis. *z* Axis lines are drawn orthogonal to the *y* axis (LRC line), and thus represent coronal planes at the level of the lambda (l), bregma (b), rcs, or nasal (n) junctions. Scale bar is shown. (B) 3D surface view of the dorsal skull showing details of skull geometry as a guide for surgical planning. Shown are axis intersections for the lambda (l), bregma (b), rcs, and nasal (n) junctions based upon orientation of the LRC line, filled circle, 0,0,0 axes origin. (C) Example of visualization of a stereotactic atlas showing brain and dorsal skull using Display. Axes show position at origin (0,0,0).

lack the morphologic information necessary for any stereotactic procedure. As such, these studies similarly do not address issues of comparative axial alignments, their definitions, or the assignment of a unitary coordinate system. While these definitions are not directly required for analysis of isolated brains using MRI; we have found that even these studies benefit from unitary coordinate definitions, particularly with respect to the quantitative/qualitative description of comparative neural defects between groups.

In our present study, we have focused on developing working atlases for two genetically important strains, C57Bl/6J and 129S1/SvImJ. Both strains are well-charac-

terized, C57Bl due in part to its role as a primary genetic background for a large number of neurologic mutations, 129Sv because of its dominant role in the development of embryonic stem cell lineages. At present, the genomes of both strains have been fully sequenced, and both strains are major targets of ethyl-nitroso urea (ENU)-based mutagenesis programs throughout the world. Atlases of these strains should thus be of benefit to a large number of researchers working on murine neuroanatomy/models of human disease.

To maximize the general utility of our stereotactic atlases, we examined the brain and skull morphology of individuals from a series of inbred and outbred *Mus musculus* strains, and we determined an optimal set of landmarks which could be utilized as a basis for comparative analyses of murine heads among different genotypic groups. With respect to delineating brain orientation, we found the most consistent landmarks to be the lambda suture junction, and the rostral confluence of the venous sinus, caudal to the olfactory bulb. We found that use of these landmarks to determine *y* axis angulation, produced alignments of the head which showed less specimen to specimen variability with respect to placements at a given CNS site, and were more consistent between strains; than previously described landmark systems. Within the lambda/RCS alignment, we have identified the dorsal most aspect of the RCS landmark as the origin for our cranial alignments (0,0,0).

With respect to the global alignment of MR scans from isolated brain specimens, these can clearly be oriented in any manner due to the digital nature of the data. However, for purposes of convenience, and due to the closer proximity of the LRC line to the natural planar aspect of the murine brain/skull (see Fig. 6) compared with the lambda/bregma, we have found it beneficial to use the stereotactic alignment parameters for analysis of all of our MR scans. We have also found this orientation helpful when comparing 3D data to histologic 2D image sets, as whole brains tend to be embedded using the flat aspect of the dorsal brain as an embedding cue. In this process the 3D dataset is utilized as a "spatial backbone" onto which higher resolution histologic sections are overlaid in an orientation which is close, or equivalent to, that indicated by the LRC line. In this regard, one group has begun to create such a multi-modal brain atlas based on MRI and histology, as well as other imaging techniques (MacKenzie-Graham et al., 2004).

The superiority of utilizing LCS/lambda over bregma/lambda to localize stereotactic structures within the brain relates to its greater stability in assigning the angulation of the horizontal axis. The stability is achieved by the increased ability of these fiduciary coordinates in sampling the single greatest source of error in the assignment of horizontal angulation; individual and sub-strain differences in dorsal skull curvature. This situation is somewhat analogous to the differential sensitivity of global positioning systems (GPS) to changes in X, Y and Z coordinates. GPS routinely provides highly reliable measures of relative longitude and latitude (XY dimension). However, accuracy in the *z* axis dimension (altitude/horizontal angulation) tends to be less reliable due to the geometric relationship of the individual (stereotactic target) to coordinating satellites (dorsal fiduciary landmarks). By increasing the separation distance between stable dorsal skull landmarks, the stability/reproducibility of horizontal angulation between individuals is increased, and the effects of local deviations in skull curvature on this measure are reduced. In addition, because the LC sinus forms beneath the skull at the rostral interface of the cerebral cortex and the olfactory bulb appearing in an equivalent manner in all murine lines examined (inbred: C57Bl6/J, 129Sv sublines, FVB/N, DBA, C3H, outbred CD1, ICR, BalbC, 129/C57 F1 intercross) as an essentially straight-line which crosses the brain midline, it acts as a landmark of the brain itself. In contrast, formation of a bregmal suture is not tied to the brain per se, and by its nature contains stochastic irregularities along its junction with each of the three cranial plates which comprise it.

The development of interactive 3D surgical atlases of the murine brain and skull will be particularly useful in advancing work on surgical models which require accurate "off-axis" stereotactic approaches to their target; further expanding the utility of the mouse as a surgical model. In traditional rodent stereotactic procedures, placements are made largely by viewing the dorsal aspect of the skull essentially as a flat X–Y plane. The development of interactive 3D models of the murine head means that one can now approach a given target from a much wider potential area with a high degree of accuracy to perform needed placements. Such procedures are becoming increasingly necessary in techniques such as *in vivo* micro-electroporation, in which DNA is introduced between two precisely placed microelectrodes. Information on the primary data files, aligned as indicated above, and related distribution information for C57Bl/6J and 129S1/SvImJ can be found at: www.phm.utoronto.ca/~jeffh/surgical.htm. Files can be accessed on any reader capable of reading MINC (*.mnc) format files.

Acknowledgments—We are indebted to N. Lifshitz, and J. Bishop and L. Yu for technical assistance. This work was supported by grants from Canadian Institute for Health Research to J.T.H and M.H., from the Ontario Research Development Challenge Fund to R.M.H; and a NARSAD Young Investigator award to J.T.H.

REFERENCES

Benveniste H, Kim K, Zhang L, Johnson GA (2000) Magnetic resonance microscopy of the C57BL mouse brain. Neuroimage 11: 601–611.

Boone JM, Velazquez O, Cherry SR, Recinos RF, Hanger CC, Schaefer RB, Dawson CA, Gosain AK (2004) Small-animal X-ray dose from micro-CT microfocal CT: a method for evaluating murine cranial sutures in situ. Mol Imaging 3:149–158.

Chen XJ, Kovacevic N, Lobaugh NJ, Sled JG, Henkelman RM, Henderson JT (2005) Neuroanatomical differences between mouse strains as shown by high-resolution 3D MRI. Neuroimage 29: 99–105.

Dhenain M, Ruffins SW, Jacobs RE (2001) Three-dimensional digital mouse atlas using high-resolution MRI. Dev Biol 232:458–470.

Ford-Hutchinson AF, Cooper DM, Hallgrimsson B, Jirik FR (2003) Imaging skeletal pathology in mutant mice by microcomputed tomography. J Rheumatol 30:2659–2665.

Franklin KBJ, Paxinos G (1997) The mouse brain in stereotaxic coordinates. San Diego: Academic Press.

Ghosh P, O'Dell M, Narasimhan PT, Fraser SE, Jacobs RE (1994) Mouse lemur microscopic MRI brain atlas. Neuroimage 1: 345–349.

Guilfoyle DN, Helpern JA, Lim KO (2003) Diffusion tensor imaging in fixed brain tissue at 7.0 T. NMR Biomed 16:77–81.

Johnson GA, Cofer GP, Gewalt SL, Hedlund LW (2002) Morphologic phenotyping with MR microscopy: the visible mouse. Radiology 222:789–793.

Kaufman MH, Brune RM, Davidson DR, Baldock RA (1998) Computer-generated three-dimensional reconstructions of serially sectioned mouse embryos. J Anat 193 (Pt 3):323–336.

Koshibu K, Levitt P, Ahrens ET (2004) Sex-specific, postpuberty changes in mouse brain structures revealed by three-dimensional magnetic resonance microscopy. Neuroimage 22:1636–1645.

Kovacevic N, Henderson JT, Chan E, Lifshitz N, Bishop J, Evans AC, Henkelman RM, Chen XJ (2005) A three-dimensional MRI atlas of the mouse brain with estimates of the average and variability. Cereb Cortex 15(5):639–645.

Ma Y, Hof PR, Grant SC, Blackband SJ, Bennett R, Slatest L, McGuigan MD, Benveniste H (2005) A three-dimensional digital atlas database of the adult C57BL/6J mouse brain by magnetic resonance microscopy. Neuroscience 135(4):1203–1215. Epub 2005 Sept. 13.

MacKenzie-Graham A, Jones ES, Shattuck DW, Dinov ID, Bota M, Toga AW (2003) The informatics of a C57BL/6J mouse brain atlas. Neuroinformatics 1:397–410.

MacKenzie-Graham A, Lee EF, Dinov ID, Bota M, Shattuck DW, Ruffins S, Yuan H, Konstantinidis F, Pitiot A, Ding Y, et al. (2004) A multimodal, multidimensional atlas of the C57BL/6J mouse brain. J Anat 204:93–102.

Messier C, Emond S, Ethier K (1999) New techniques in stereotaxic surgery and anesthesia in the mouse. Pharmacol Biochem Behav 63:313–318.

Munasinghe JP, Gresham GA, Carpenter TA, Hall LD (1995) Magnetic resonance imaging of the normal mouse brain: comparison with histologic sections. Lab Anim Sci 45:674–679.

Natt O, Watanabe T, Boretius S, Radulovic J, Frahm J, Michaelis T (2002) High-resolution 3D MRI of mouse brain reveals small cerebral structures in vivo. J Neurosci Methods 120:203–209.

Paxinos G, Watson C (1986) The rat brain in stereotactic coordinates, 2nd ed. Sydney: Academic Press.

Recinos RF, Hanger CC, Schaefer RB, Dawson CA, Gosain AK (2004) Microfocal CT: a method for evaluating murine cranial sutures in situ. J Surg Res 116:322–329.

Rogers WT, Moser AR, Schwaber JS (1990) Digital brain atlas for anatomical data comparison and integration. In: Three dimensional neuroimaging (Toga AW, ed), pp 123–124. New York: Raven Press Ltd.

Santori EM, Toga AW (1993) Superpositioning of three dimensional neuroanatomic data sets. J Neurosci Methods 50:187–196.

Slotnik BM, Leonard CM (1975) A stereotactic atlas of albino mouse forebrain. Rockville, MD: US Department of Health, Education and Welfare.

(Accepted 31 August 2006)
(Available online 13 November 2006)